Unintegrated parton density functions

John Collins[1], *Markus Diehl*[2], *Hannes Jung*[2], *Leif Lönnblad*[3], *Michael Lublinsky*[4], *Thomas Teubner*[5]
[1] Physics Department,Penn State University, U.S.A.
[2] Deutsches Elektronen-Synchroton Hamburg, FRG
[3] Department of Theoretical Physics, Lund University, Sweden
[4] University of Connecticut, U.S.A.
[5] University of Liverpool, U.K

Abstract

An overview on activities to determine unintegrated parton density functions is given and the concept and need for unintegrated PDFs is discussed. It is also argued that it is important to reformulate perturbative QCD results in terms of fully unintegrated parton densities, differential in all components of the parton momentum. Also the need for non-linear BFKL evolution is discussed and results using the BK equation supplemented by DGLAP corrections at short distances is reviewed. Finally the use unintegrated generalized parton distributions for hard diffractive processes is discussed.

1 Unintegrated parton density functions[1]

The parton distributions of hadrons still cannot be calculated from first principles, but have to be determined experimentally. However, once the initial distributions $f_i^0(x, \mu_0^2)$ at the hadronic scale ($\mu^2 \sim 1\,\text{GeV}^2$) are determined, different approximations allow to calculate the parton density functions (PDFs) for different kinematic regions:

- DGLAP [1–4] describes the evolution with the scale μ^2
- BFKL [5–7] describes the evolution in the longitudinal momenta x
- CCFM [8–11] describes the evolution in an angular ordered region of phase space while reproducing DGLAP and BFKL in the appropriate asymptotic limits

The different evolution equations attempt to describe different regions of phase space on the basis of in perturbative QCD (pQCD).

1.1 Introduction to uPDFs and $k_\perp$ factorization

In the collinear factorization ansatz the cross sections are described by x-dependent density functions $f_i(x, \mu^2)$ of parton i at a given factorization scale μ convoluted with an (on-shell) coefficient function (matrix element):

$$\sigma(a + b \rightarrow X) = \int dx_1 dx_2 f_i(x_1, \mu^2) f_j(x_2, \mu^2) \hat{\sigma}_{ij}(x_1, x_2, \mu^2) \tag{1}$$

with $\hat{\sigma}_{ij}(x_1, x_2, \mu^2)$ being the hard scattering process for the partons $i + j \rightarrow X$. In this equation we have left implicit all external kinematic variables, keeping only the variables used in the parton densities. This ansatz is very successful in describing inclusive cross sections, such as the structure function $F_2(x, Q^2)$ at HERA or the inclusive production of vector bosons or Drell-Yan in proton proton collisions. The free parameters of the starting distributions $f_i^0(x, \mu_0^2)$ are determined such that after a DGLAP evolution to the scale $\mu^2 = Q^2$ and convolution with the coefficient functions the measured structure function

---

[1]Authors: Hannes Jung and Leif Lönnblad.

$F_2(x, Q^2)$ at HERA (and, usually, some other cross sections, e.g., in hadron-hadron and neutrino-hadron scattering) are best described.

However, as soon as, for example, final-state processes are considered, the collinear factorization ansatz becomes more and more unreliable, because neglecting the transverse momenta of the partons during the (DGLAP) evolution leads to inconsistencies, as will be discussed in more detail in section 2. Collinear factorization is only appropriate when (a) the transverse momentum (and virtuality) of the struck parton(s) can be neglected with respect to Q, and (b) the integrals over these variables can be treated as independent and unrestricted up to the scale Q. (Certain complications concerning high transverse momentum partons are correctly treated by NLO and higher corrections to the hard scattering.) When these requirements are not met, a more general treatment using unintegrated parton densities (uPDFs) is better.

For example, in the small x regime, when the transverse momenta of the partons are of the same order as their longitudinal momenta, the collinear approximation is no longer appropriate and high energy or $k_\perp$ - factorization has to applied, with the appropriate BFKL or CCFM evolution equations. Cross sections are then $k_\perp$- factorized [12–15] into an off-mass-shell ($k_\perp$- dependent) partonic cross section $\hat{\sigma}(x_1, x_2, k_{\perp 1}, k_{\perp 2})$ and a $k_\perp$- unintegrated parton density function (uPDF) $\mathcal{F}(z, k_\perp)$:

$$\sigma = \int dx_1 dx_2 d^2 k_{\perp 1} d^2 k_{\perp 2} \hat{\sigma}_{ij}(x_1, x_2, k_{\perp 1}, k_{\perp 2}) \mathcal{F}(x_1, k_{\perp 1}) \mathcal{F}(x_2, k_{\perp 2}) \tag{2}$$

The unintegrated gluon density $\mathcal{F}(z, k_\perp)$ is described by the BFKL evolution equation in the region of asymptotically large energies (small x). It is important to note that only when the $k_\perp$ dependence of the hard scattering process $\hat{\sigma}$ can be neglected, i.e. if $\hat{\sigma}(x_1, x_2, k_{\perp 1}, k_{\perp 2}) \sim \hat{\sigma}(x_1, x_2, 0, 0)$, then the $k_\perp$ integration can be factorized and an expression formally similar to eq.(1) is obtained.

An appropriate description valid for both small and large x, is given by the CCFM evolution equation, resulting in an unintegrated gluon density $\mathcal{A}(x, k_\perp, \mu)$, which is a function also of the additional evolution scale μ. This scale is connected to the factorization scale in the collinear approach.

Further examples where uPDFs are needed are the Drell-Yan and related processes at low transverse momentum, as in the CSS formalism [16]. However, the relation between CSS method (which does not need small x) and $k_\perp$-factorization of the BFKL/CCFM kind (for small x) has not yet been properly worked out.

1.2 Extraction and determination of uPDFs

In this section we will review how measurements of uPDFs have been extracted from DIS data at small x, mostly from the inclusive structure function F_2. For measurements of the uPDFs in Drell-Yan processes using the CSS formalism, see [17].

From the DIS data, the uPDF can be obtained by adjusting the non-perturbative input distribution $f_i^0(x, \mu_0^2)$ and the free parameters of the perturbative evolution such that after convolution with the appropriate off-shell matrix element (according to eq.(2)) a measured cross section is best described.

Applying $k_\perp$-factorization to determine the uPDF from DIS data until now mainly the inclusive structure function measurements of $F_2(x, Q^2)$ at HERA have been used. The exceptions are those which are simply derivatives of integrated PDFs, which then neglects fully the transverse momentum dependence of the matrix element. Extracting a uPDF from the integrated PDF is appropriate only if the $k_\perp$-dependence of the hard scattering process $\hat{\sigma}$ in eq.(2) can be neglected. In addition, contributions from $k_\perp > \mu$, which are present in a full calculation, are entirely neglected. It thus can only provide an estimate of the proper kinematics in the collinear approach, which is otherwise fully neglected when using integrated PDFs.
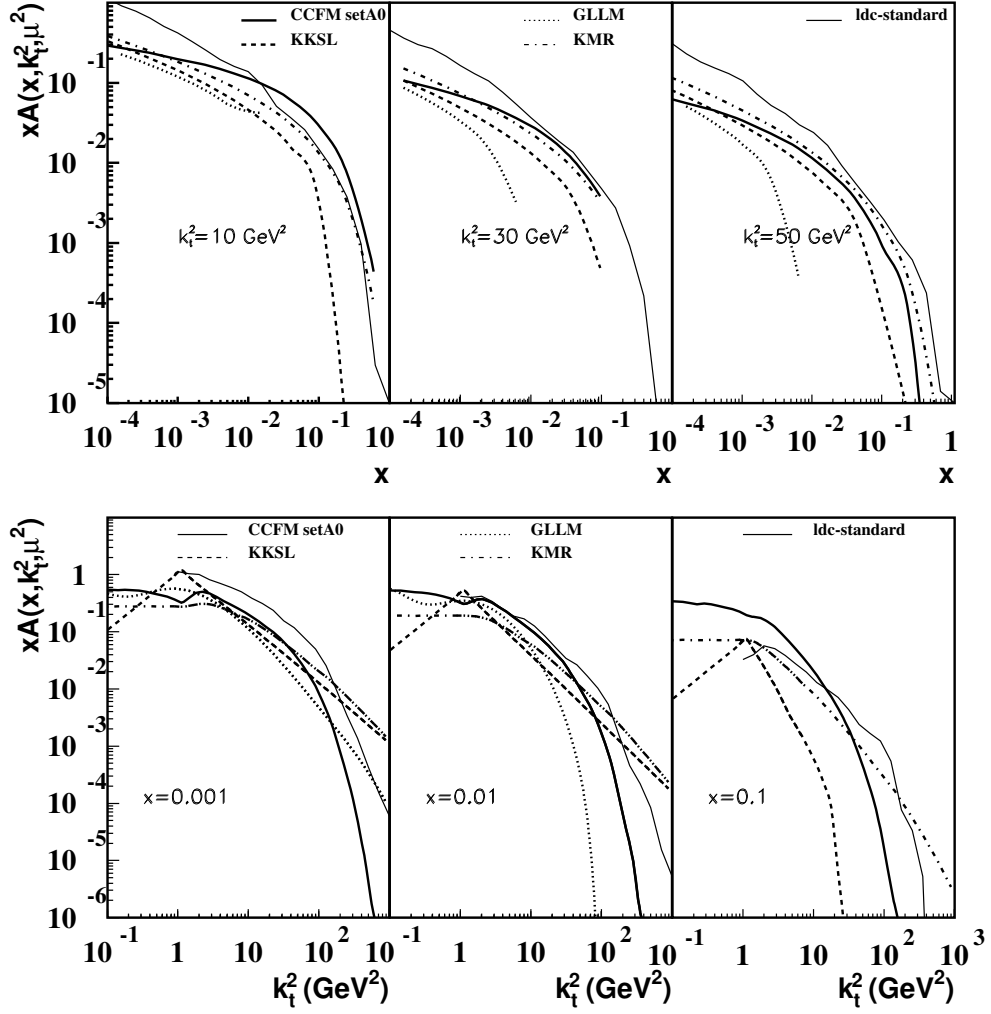
Fig. 1: Comparison of different uPDFs at $\mu = 10$ GeV.

Here we compare some of these parameterizations which have been obtained in different ways:

– **CCFM set A0** was obtained using CCFM evolution in [18, 19].

– **LDC standard** was similarly obtained in [20] using LDC evolution [21], which is a reformulation and generalization of CCFM.

– **KKSL** [22] was obtained from a combined BFKL and DGLAP evolution following [23].

– **GLLM** [24] was obtained applying the BK equation to HERA F_2 measurements, as described in Section 3.

– **KMR** is one of the more advanced derivatives of integrated PDFs, using Sudakov form factors [25].

In Fig. 1 we show a comparison of the different uPDFs as a function of x and $k_\perp$ at a factorization scale $\mu = 10$ GeV. All the parameterizations are able to describe the measured $F_2(x, Q^2)$ in the small x range reasonably well, with a $\chi^2/ndf \sim 1$. In Fig. 2 the same uPDFs are compared at a factorization scale which is relevant at LHC energies, e.g. for inclusive Higgs production ($\mu = 120$ GeV). One should note that the uPDFs from KKSL and GLLM have no explicit factorization scale dependence, therefore they are the same as in Fig 1.

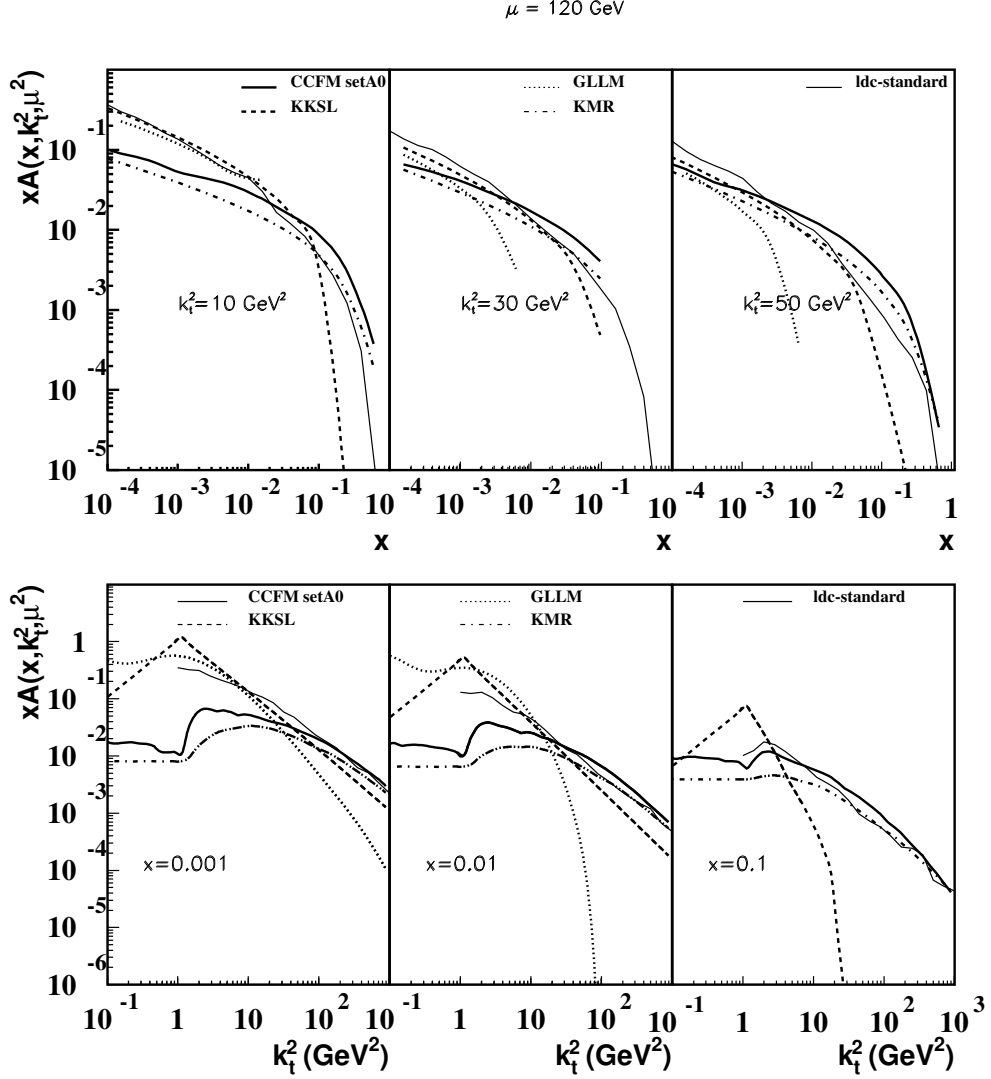**Fig. 2:** Comparison of different uPDFs at $\mu = 120$ GeV.

1.3 Extrapolation to LHC energies

All the parameterizations of uPDFs considered in this report give a fairly good fit to HERA F_2 data. This means that they are well constrained mainly in the region of small x and relatively small Q^2, where the bulk of the HERA data is concentrated. For higher x and Q^2, a fit to HERA data is less constraining, and indeed some of the parameterizations based on the CCFM and LDC evolution of the gluon alone are only fitted in the small-x region (typically $x < 0.01$, $Q^2 < 100$ GeV^2).

When evolving the uPDFs to apply them to the processes of main interest at the LHC, such as Higgs production, this is a serious concern. Although the x-values in such processes are typically below 0.01, the scales involved are of the order of 10^4 GeV^2 or more. Through the evolution one then becomes sensitive to larger x-values at lower scales where the current parameterizations are less constrained.

A notable exception is the KMR [25] densities which are obtained from a global fit of integrated PDFs, which should give reliable prediction at LHC at least for integrated observables such as the inclusive Higgs cross section. In contrast, it was shown in [20] that the CCFM [8–11] and LDC [21] evolved uPDFs have unreasonably large uncertainties for such cross sections. On the other hand it was also shown in [20] that there are some questions about the constraint of the actual $k_\perp$ distribution of the KMR uPDFs resulting eg. in a too soft $p_\perp$ spectrum of W or Z production at the Tevatron for small transverse
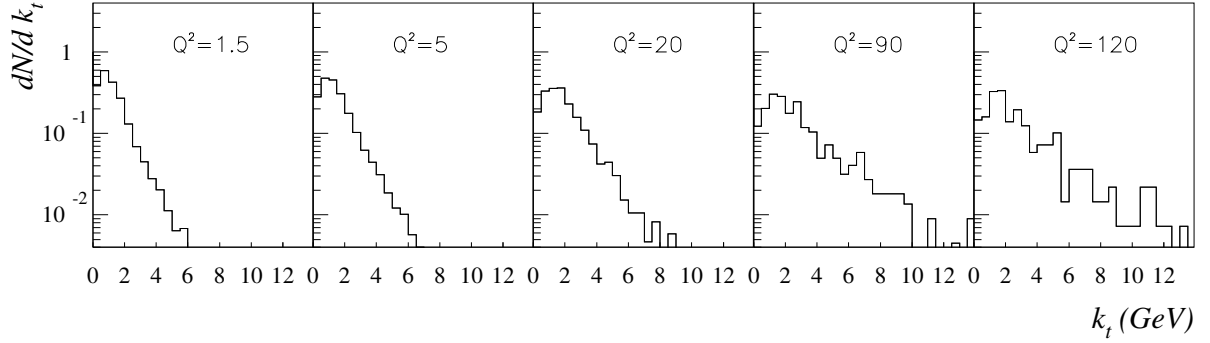
Fig. 3: $k_\perp$ distribution in different Q^2 bins used in $F_2(x, Q^2)$ at HERA.
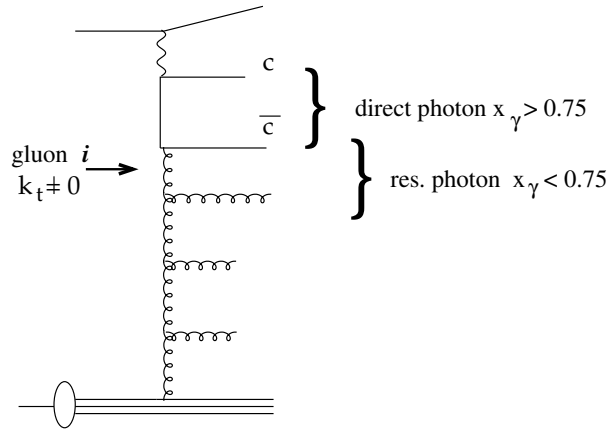
**Fig. 4:** Diagram of charm photoproduction, showing the sensitivity to the gluon transverse momentum

momenta. Hence, although the KMR prediction for inclusive quantities may be reliable at the LHC, the predictions of eg. the detailed distribution of low-$p_\perp$ Higgs may be questionable.

What is needed is clearly to obtain fits of the uPDFs, not only to HERA F_2 data, but also to observables more sensitive to higher x and Q^2 values, as well as to observables directly sensitive to the $k_\perp$ distribution. To obtain such global fits there is a need for both theoretical and phenomenological developments. Examples of the former is the inclusion of quarks in the CCFM evolution, while the latter involves the development of $k_\perp$-sensitive observables, where HERA data at small x, such as forward jet or heavy quark production, will play an important role, as discussed in the following.

1.4 Global uPDF fits

Until now the uPDFs obtained from DIS were only determined and constrained by the inclusive structure function $F_2(x, Q^2)$. It is clear that the inclusive measurements are not very sensitive to the details of the $k_\perp$ dependence. In Fig. 3 we show the $k_\perp$ distribution of the gluon in $\gamma^* g^* \to q\bar{q}$ which is the relevant process for F_2 at small x. The $k_\perp$-distributions in Fig. 3 are obtained with CASCADE [26, 27] using the CCFM uPDFs. The bins in Q^2 are typical for HERA F_2 measurements. It is interesting to observe that even at large Q^2 essentially only the small $k_\perp$ region is probed by F_2.

A larger lever arm for the $k_\perp$ distribution can be obtained with photoproduction of $D^* +$ jet events at HERA. In Fig. 4 the relevant diagram is shown. The quantity x_γ, normally designed to separate direct from resolved photon processes, can be also used to distinguish small and large $k_\perp$- regions. The region of large x_γ corresponds to measuring jets coming from the quark-box. The region of small x_γ
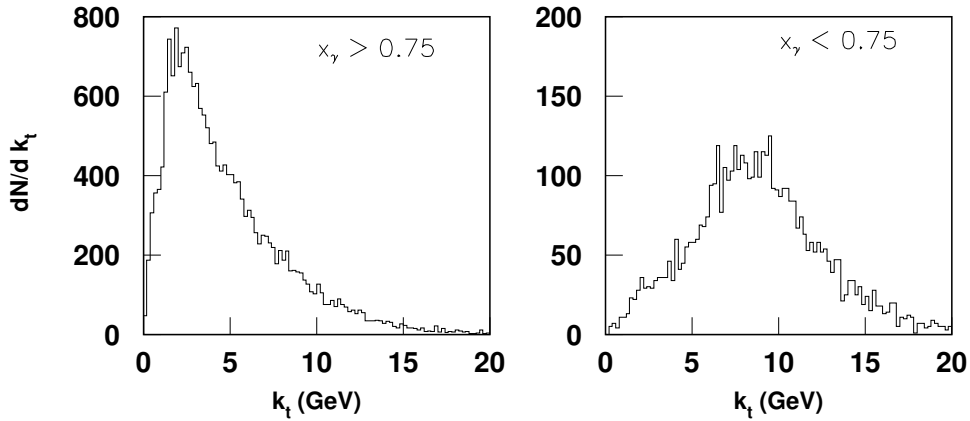
Fig. 5: $k_\perp$ distribution in different x_γ bins obtained from D^*+jet photo-production at HERA.

corresponds to the situation where one of the jets originates from a gluon, as indicated in Fig. 4. Thus, the transverse momentum of the gluon i can be probed, as shown in Fig. 5 for two different regions of x_γ using CASCADE . It is interesting to note that the average $k_\perp$ distribution for bottom production at the Tevatron is similar to what it shown in Fig. 5.

To further constrain the uPDF it would be desirable to perform a common fit to inclusive measurements like F_2 and simultaneously to final state measurements.

Once the data sets and the sensitivity to the uPDFs have been identified, a systematic error treatment of the data used in the uPDF fits can be performed. Until now, the uPDFs are not really the result of a fit but rather a proof that the uPDF is consistent with various measurements.

A uPDF fit would require a systematic variation of the parameters used to specify the non-perturbative input gluon distribution as well as a systematic treatment of the experimental systematic uncertainties. Only then an uncertainty band of the uPDFs can be given. To consider the uncertainty of the uPDF given from the spread of different available parameterizations is a very rough estimate.

1.5 Outlook and Summary

Clearly, the extraction of uPDFs from data is still in its infancy, especially if compared to the well developed industry of fitting integrated PDFs. The uPDFs are only leading order parameterizations, they have mainly been fitted to F_2 data at small x, and besides the KMR and LDC parameterizations, no attempts have been made to obtain unintegrated quark densities. Taken together, this means that the applicability to LHC processes are uncertain. However, the field is maturing and we hope to soon be able to do more global uPDF fits which will greatly enhance the reliability of the predictions for the LHC. In doing so the small-x data from HERA will be very important, but also eg. Tevatron data will be able to provide important constraints.

2 Need for fully unintegrated parton densities[2]

2.1 Introduction

Conventional parton densities are defined in terms of an integral over all transverse momentum and virtuality for a parton that initiates a hard scattering. While such a definition of an integrated parton density is appropriate for very inclusive quantities, such as the ordinary structure functions F_1 and F_2 in DIS, the definition becomes increasingly unsuitable as one studies less inclusive cross sections. Associated

---

[2]Authors: John Collins and Hannes Jung.
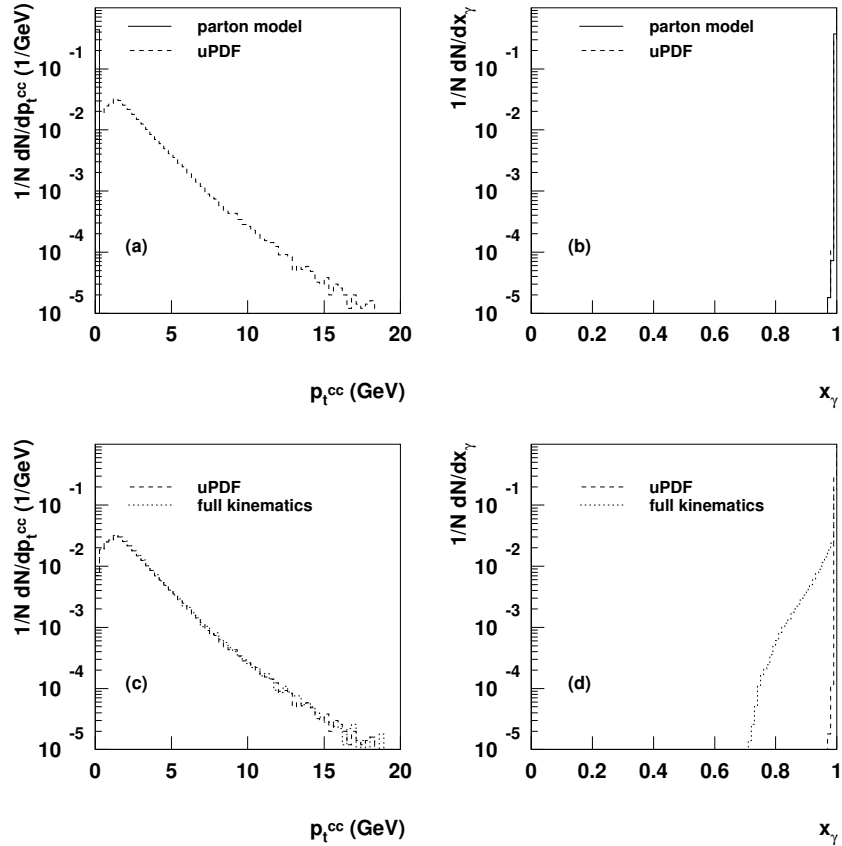
Fig. 6: (a) and (b): comparison between use of simple LO parton model approximation and of the use of $k_\perp$ densities for the p_T of $c\bar{c}$ pairs in photoproduction, and for the x_γ. (c) and (d): comparison of use of $k_\perp$ densities and full simulation.

with the use of integrated parton densities are approximations on parton kinematics that can readily lead to unphysical cross sections when enough details of the final state are investigated.

We propose that it is important to the future use of pQCD that a systematic program be undertaken to reformulate factorization results in terms of fully unintegrated densities, which are differential in both transverse momentum and virtuality. These densities are called "doubly unintegrated parton densities" by Watt, Martin and Ryskin [28, 29], and "parton correlation functions" by Collins and Zu [30]; these authors have presented the reasoning for the inadequacy, in different contexts, of the more conventional approach. The new methods have their motivation in contexts such as Monte-Carlo event generators where final-state kinematics are studied in detail. Even so, a systematic reformulation for other processes to use unintegrated densities would present a unified methodology.

These methods form an extension of $k_\perp$-factorization. See Sec. 1 for a review of $k_\perp$-factorization, which currently involves two different formalisms, the BFKL/CCFM methods [5–11] and the CSS method [16].

2.2 Inadequacy of conventional PDFs

The problem that is addressed is nicely illustrated by considering photoproduction of $c\bar{c}$ pairs. In Figs. 6, we compare three methods of calculation carried out within the CASCADE event generator [26, 27]:

- Use of a conventional gluon density that is a function of parton x alone.
- Use of a $k_\perp$ density that is a function of parton x and $k_\perp$. These are the "unintegrated parton densities" (uPDFs) that are discussed in Sec. 1

7
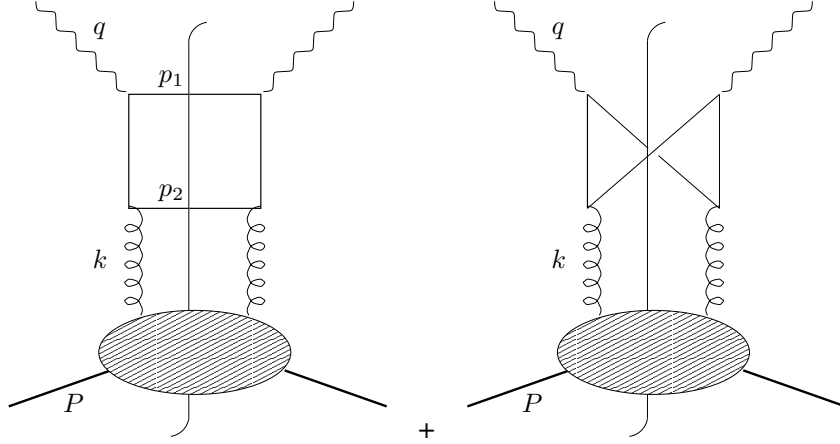
Fig. 7: Photon-gluon fusion.

- Use of a doubly unintegrated density that is a function of parton x, $k_\perp$ and virtuality, that is, of the complete parton 4-momentum.

The partonic subprocess in all cases is the lowest order photon-gluon-fusion process $\gamma + g \longrightarrow c + \bar{c}$ (Fig. 7). Two differential cross sections are plotted: one as a function of the transverse momentum of the $c\bar{c}$ pair, and the other as a function of the x_γ of the pair. By x_γ is meant the fractional momentum of the photon carried by the $c\bar{c}$ pair, calculated in the light-front sense as

$$x_\gamma = \frac{\sum_{i=c,\bar{c}}(E_i - p_{z\,i})}{2yE_e} = \frac{p_{c\bar{c}}^-}{q^-}.$$

Here E_e is the electron beam energy and the coordinates are oriented so that the electron and proton beams are in the $-z$ and $+z$ directions respectively.

In the normal parton model approximation for the hard scattering, the gluon is assigned zero transverse momentum and virtuality, so that the cross section is restricted to $p_{Tc\bar{c}} = 0$ and $x_\gamma = 1$, as shown by the solid lines in Fig. 6(a,b). When a $k_\perp$ dependent gluon density is used, quite large gluonic $k_\perp$ can be generated, so that the $p_{Tc\bar{c}}$ distribution is spread out in a much more physical way, as given by the dashed line in Fig. 6(a). But as shown in plot (b), x_γ stays close to unity. Neglecting the full recoil mass $m_{\rm rem}$ (produced in the shaded subgraph in Fig 7) is equivalent of taking $k^2 = -k_\perp^2/(1-x)$ with k^2 being the virtuality of the gluon in Fig. 7, $k_\perp$ its transverse momentum and x its light cone energy fraction. This gives a particular value to the gluon's k^-. When we also take into account the correct virtuality of gluon, there is no noticeable change in the $p_{Tc\bar{c}}$ distribution — see Fig. 6(c) (dashed line) — since that is already made broad by the transverse momentum of the gluon. But the gluon's k^- is able to spread out the x_γ distribution, as in Fig. 6(d) with the dashed line. This is equivalent with a proper treatment of the kinematics and results in $k^2 = -(k_\perp^2 + xm_{\rm rem}^2)/(1-x)$, where $m_{\rm rem}$ is the invariant mass of the beam remnant, the part of the final state in the shaded blob in Fig. 7. This change can be particularly significant if x is not very small.

Note that if partons are assigned approximated 4-momenta during generation of an event in a MC event generator, the momenta need to be reassigned later, to produce an event that conserves total 4-momentum. The prescription for the reassignment is somewhat arbitrary, and it is far from obvious what constitutes a correct prescription, especially when the partons are far from a collinear limit. A treatment with fully unintegrated PDFs should solve these problems.

If, as we claim, an incorrect treatment of parton kinematics changes certain measurable cross sections by large amounts, then we should verify directly that there are large discrepancies in the distributions in partonic variables themselves. We see this in Fig. 8. Graph (a) plots the gluonic transverse

8
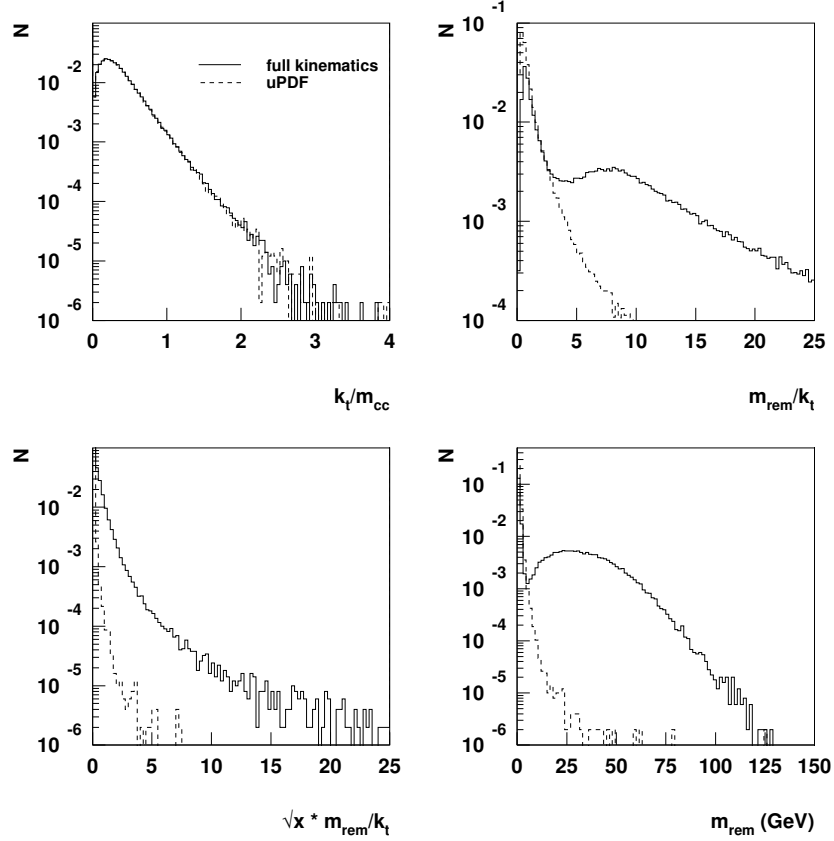
Fig. 8: Comparison of distributions in partonic variables between calculations with full parton kinematics and with ordinary unintegrated PDFs.

momentum divided by the charm-pair mass. As is to be expected, the typical values are less than one, but there is a long tail to high values. But the use of full parton kinematics does not have much of an effect, the unintegrated parton distributions already providing realistic distributions in transverse momentum.

On the other hand, a simple collinear approximation for showering sets the remnant mass, m_{rem}, to zero. As can be seen from the formulae for the gluon virtuality, this only provides a good approximation to the gluon kinematics if m_{rem} is much less than $k_{\perp}$. In reality, as we see from graph (b), there is a long tail to large values of $m_{\mathrm{rem}}/k_{\perp}$, and the tail is much bigger when correct kinematics are used. A more correct comparison uses $x m_{\mathrm{rem}}^2$, with an extra factor of x. Even then, there is a large effect, shown in graph (c). The vertical scale is logarithmic, so the absolute numbers of events are relatively small, but the tail is broad. Finally, graph (d) shows that the distribution in m_{rem} itself is very broad, extending to many tens of GeV. This again supports the argument that unless a correct treatment of parton kinematics is made, very incorrect results are easily obtained.

It is important to note that, for the cross sections themselves, the kinematic variables used in Fig. 6 are normal ones that are in common use. Many other examples are easily constructed. Clearly, the use of the simple parton-model kinematic approximation gives unphysically narrow distributions. The correct physical situation is that the gluon surely has a distribution in transverse momentum and virtuality, and for the considered cross sections neglect of parton transverse momentum and virtuality leads to wrong results. It is clearly better to have a correct starting point even at LO, for differential cross sections such as we have plotted.

2.3 Kinematic approximations

The standard treatment of parton kinematics involves replacing the incoming parton momentum k by its plus component only: $k^\mu \mapsto \hat{k}^\mu \equiv (k^+, 0, 0_T)$. There are actually two parts to this. The first is to neglect the $^-$ and transverse components of k with respect to the large transverse momenta in the calculation of the numerical value of the hard-scattering amplitude; this is a legitimate approximation, readily corrected by higher order terms in the hard scattering. The second part is to change the kinematics of the final-state particles, p_1 and p_2, so that their sum is q plus the approximated gluon momentum. It is this second part that is problematic, for it amounts to the replacement of the momentum conservation delta function $\delta^{(4)}(k + q - p_1 - p_2)$ by $\delta^{(4)}(\hat{k} + q - p_1 - p_2)$. These delta-functions are infinitely different, point-by-point. Only when integrated with a sufficiently smooth test function can they be regarded as being approximately the same, as in a fully inclusive cross section.

In an event generator, the effect is to break momentum conservation, which is restored by an ad hoc correction of the parton kinematics. Note that the change of parton kinematics is only in the hard scattering, i.e., in the upper parts of the graphs. Parton kinematics are left unaltered within the parton density part, and the integrals over $k_\perp$ and virtuality are part of the standard definition of integrated PDFs.

The situation is ameliorated by inclusion of NLO terms, and perhaps also by some kind of resummation. But these do not correct the initial errors in the approximation, and lead to a very restricted sense in which the derivation of the cross section can be regarded as valid. Furthermore, when much of the effect of NLO terms is to correct the kinematic approximations made in LO, this is an inefficient use of the enormous time and effort going into NLO calculations. A case in point is the BFKL equation, where 70% of the (large) NLO corrections are accounted for [31] by the correction of kinematic constraints in the LO calculation.

2.4 Conclusions

The physical reasoning for the absolute necessity of fully unintegrated densities is, we believe, unquestionable. Therefore it is highly desirable to reformulate perturbative QCD methods in terms of doubly unintegrated parton densities from the beginning. A full implementation will be able to use the full power of calculations at NLO and beyond.

Among other things, a full implementation, as in [30], will provide extra factorization formulae for obtaining the values of the unintegrated densities at large parton transverse momentum and virtuality. This will incorporate all possible perturbatively calculable information, so that the irreducible nonperturbative information, that must be obtained from data, will be at low transverse momentum and virtuality. In addition, the implementation will quantify the relations to conventional parton densities. With the most obvious definitions, the integrated PDFs are simple integrals of the unintegrated densities. However, in full QCD a number of modifications are required [30,32], so that the relations between integrated and unintegrated PDFs are distorted.

The fact that we propose new and improved methods does not invalidate old results in their domain of applicability. The work of Watt, Martin and Ryskin, and of Collins and Zu provides a start on this project; but much remains to be done to provide a complete implementation in QCD; for example, there is as yet no precise, valid, and complete gauge-invariant operator definition of the doubly unintegrated densities in a gauge theory.

The outcome of such a program should have the following results:

1. Lowest order calculations will give a kinematically much more realistic description of cross sections. This may well lead to NLO and higher corrections being much smaller numerically than they typically are at present, since the LO description will be better.

2. It will also obviate the need for separate methods (resummation or the CSS technique), which are currently applied to certain individual cross sections like the transverse-momentum distribution for the Drell-Yan process. All these and others will be subsumed and be given a unified treatment.

3. A unified treatment will be possible for both inclusive cross sections using fixed order matrix element calculations and for Monte-Carlo event generators.

4. For a long-term theoretical perspective, the doubly unintegrated distributions will interface to methods of conventional quantum many-body physics much more easily than regular parton densities, whose definitions are tuned to their use in ultra-relativistic situations.

This program is, of course, technically highly nontrivial if it is to be used in place of conventional methods with no loss of predictive power. A start is made in the cited work.

Among the main symptoms of the difficulties are that the most obvious definition of a fully unintegrated density is a matrix element of two parton fields at different space-time points, which is not gauge-invariant. It is often said that the solution is to use a light-like axial gauge $A^+ = 0$. However, in unintegrated densities, this leads to divergences — see [32] for a review — and the definitions need important modification, in such a way that a valid factorization theorem can be derived.

We also have to ask to what extent factorization can remain true in a generalized sense. Hadron-hadron collisions pose a particular problem here, because factorization needs a quite nontrivial cancellation arising from a sum over final-state interactions. This is not compatible with simple factorization for the exclusive components of the cross section, and makes a distinction between these processes and exclusive components of DIS, for example.

3 PDF extrapolation to LHC energies based on combined BK/DGLAP equations [3]

3.1 Introduction

In recent years it became clear that the DGLAP evolution is likely to fail in certain kinematics associated with the *low x* domain. This might be a dangerous problem for certain DGLAP based predictions made for the LHC. The reasons for the failure are well known.

– DGLAP predicts a very steep rise of gluon densities with energy. If not suppressed this rise will eventually violate unitarity.
– The leading twist evolution breaks down when higher twists become of the same order as the leading one. We have to recall here that higher twists are estimated to rise with energy much faster than the leading one [33].
– The DGLAP evolution is totally unable to describe physics of low photon virtualities.

It is most important to stress that NLO corrections are in principal unable to solve any of the above problems, though they can potentially help to delay their onset.

Fortunately, a solution to the low x problem does exist. We have to rely on a nonlinear evolution based on the BFKL dynamics. So far the best candidate on the market is the Balitsky-Kovchegov (BK) equation [34, 35], which is a nonlinear version of the LO BFKL equation. Compared to the DGLAP equation it has the following advantages:

– it accounts for saturation effects due to high parton densities.
– it sums higher twist contributions.
– it allows an extrapolation to large distances.

Though the BK evolution takes care of the low x domain, it misses the essential part of the short distance physics correctly accounted for by the DGLAP evolution. The reason is that the BFKL kernel

---

[3] Author: Michael Lublinsky.

involves the $1/z$ part only of the full gluon-gluon splitting function $P_{gg}(z)$. Thus we have to develop a scheme which in a consistent manner would use elements of both the equations. Such scheme was proposed in Ref. [36] and realized in a successful fit to F_2 data in Ref. [37].

One of the main problems of the DGLAP evolution is a necessity to specify the x dependence of the distributions in the initial conditions of the evolution. The scheme which we propose generally avoids this problem and thus can be used for future more elaborated analysis including NLO corrections and the quark sector.

At low x it is very convenient to use the dipole picture. In this approach the structure function F_2 can be expressed through the universal dipole cross section σ^{dipole}:

$$F_2(y, Q^2) \; = \; \frac{Q^2}{4\pi^2} \int d^2 r \int dz \, P^{\gamma^*}(Q^2; r, z) \, \sigma^{dipole}(r, y) \,. \tag{3}$$

with the probability to find a dipole of the transverse size r in the photon's wavefunction given by

$$P^{\gamma^*}(Q^2; r, z)^2 \; = \; \frac{N_c}{2\pi^2} \sum_{f=1}^{3} Z_f^2 \left\{ (z^2 + (1-z)^2) \, a^2 \, K_1^2(a\, r) \; + \; 4\, Q^2 \, z^2 \, (1-z)^2 \, K_0^2(a\, r) \right\} ,$$

where $a^2 = Q^2 z(1-z)$, Z_f are the quark charges, and K_i the standard modified Bessel functions.

The dipole cross section is determined through the evolution of the imaginary part of the dipole target elastic amplitude N subsequently integrated over the impact parameter b (in the analysis of Ref. [37] the dependence on b was modeled):

$$\sigma^{dipole}(r, y) \; = \; 2 \int d^2 b \, N(r, y; b) \,.$$

In our approach, the amplitude $\tilde{N}$ is given by a sum of two terms

$$N \; = \; \tilde{N} \, + \, \Delta N$$

The first term $\tilde{N}$ follows from the solution of the BK equation whereas ΔN is a DGLAP correction to it (Fig. 9). The strategy of the fit is the following. We trust the DGLAP evolution for x above $x_0 = 10^{-2}$. The gluon density obtained as a result of this evolution is then used as a initial condition for the low x evolution based on the BK equation. In practice the CTEQ6 gluon was used as an input. The large distance behavior was extrapolated using the method proposed in Ref. [38]. The extrapolation is based on the geometrical scaling [39], a phenomenon experimentally observed by HERA. The BK evolved function N is fitted to the low Q^2 data, with the effective proton size being the only fitting parameter entering the b dependence ansatz. As the last step, the DGLAP correction ΔN is switched on and computed by solving a DGLAP-type equation. An inhomogeneous N-dependent term in the equation acts as a source term for ΔN. This allows to have zero initial condition for the DGLAP correction. [4]

3.2 Results

We skip most of the technical details reported in Ref. [37] and present a result of the fit with $\chi^2/d.o.f. \simeq 1$. Fig. 10 displays the results vs. a combined set of experimental data for x below 10^{-2}. The solid line is the final parameterization. The dashed line on plot (b) is the result without DGLAP corrections added. Figure 11, a presents our results for the logarithmic derivative of F_2 with respect to $ln x$. This graph illustrates the hard-soft pomeron transition as a result of multiple rescattering of the BFKL pomeron. The intercept decreases from the LO BFKL intercept of the order 0.3 to the hadronic value of the order 0.1. As clearly observed from Fig. 11a, the intercept depends strongly on the photon virtuality Q^2 and decreases towards hadronic value when the virtuality decreases. If we further increase the energy, the
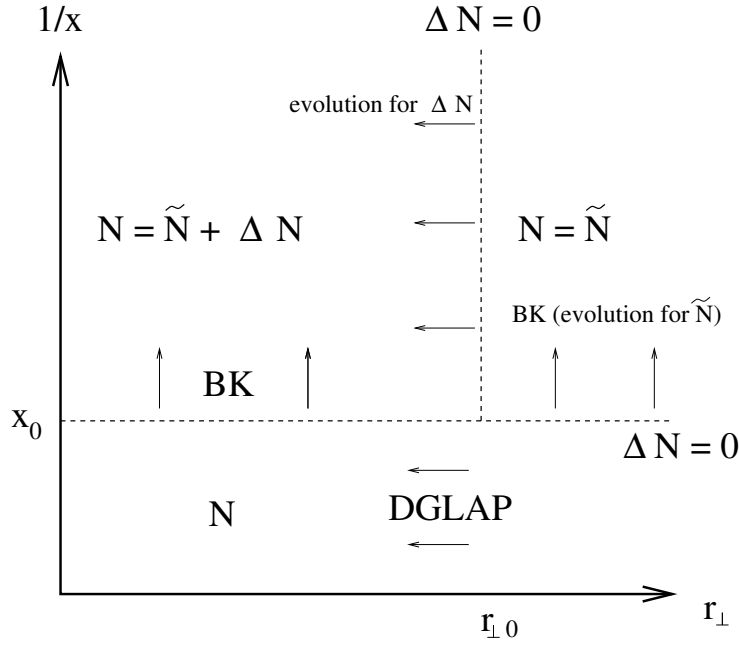
Fig. 9: The kinematic map for the solutions.
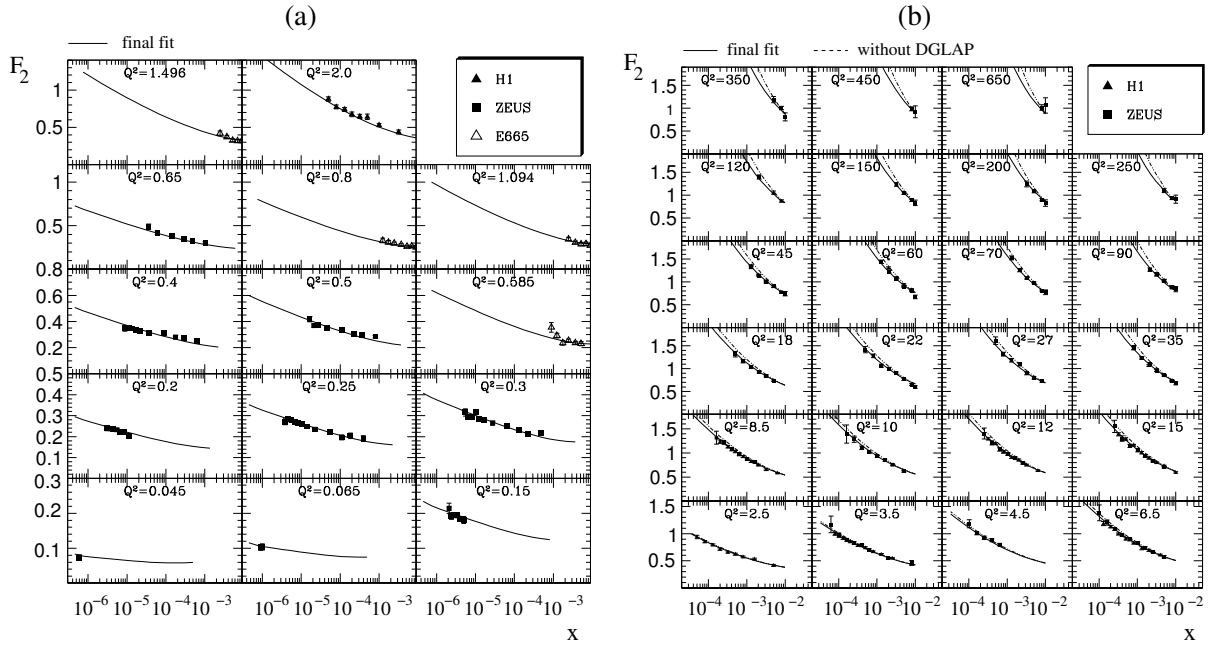
Fig. 10: Fit to the F_2 structure function.

intercept would eventually vanish in accord with the unitarity requirements. The band of our estimates for the value of saturation scale at LHC is displayed on Fig. 11b together with the most popular Golec-Biernat Wüsthoff saturation model [40]. Based on our analysis we predict much stronger saturation effects compared to the ones which could be anticipated from the GBW model. Though the power growth of the saturation scale in both cases is given by the very same exponent of the order $\lambda \simeq 0.3$, we had to take a much stronger saturation input at the beginning of the evolution.

---

[4]The initial condition for the BK equation is CTEQ gluon distribution. In the DGLAP-type equation for ΔN an initial condition at $r = r_0$ is required, which is set to zero and no modelling of the small x behavior is needed.
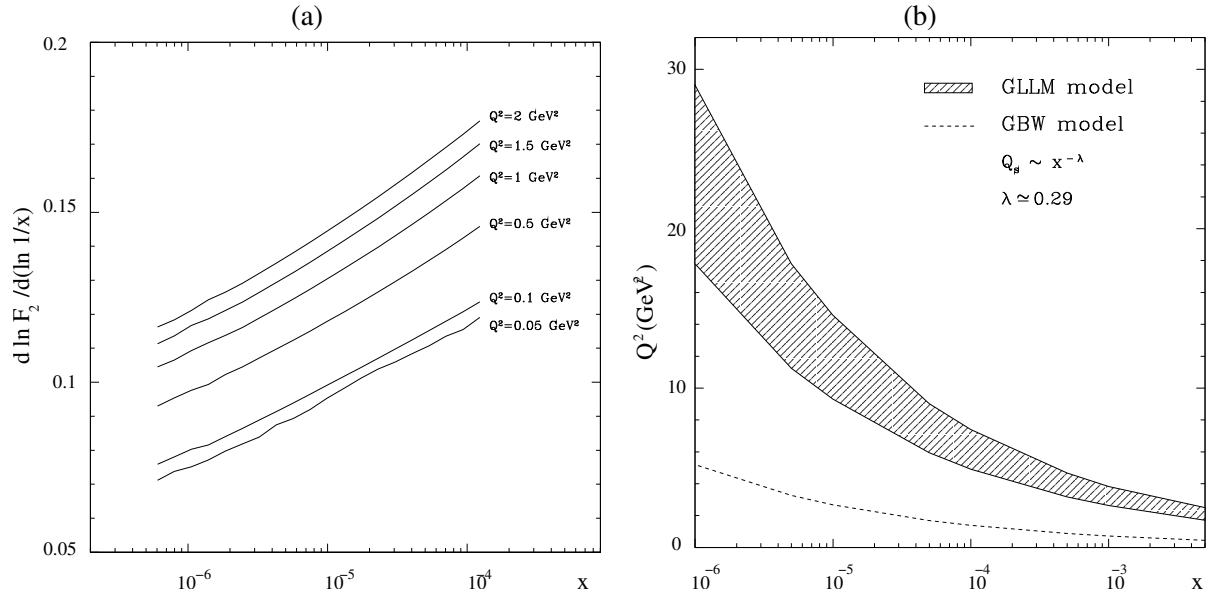
Fig. 11: (a) The logarithmic derivative $\lambda = \partial \ln F_2 / \partial \ln 1/x$ plotted at low Q^2 and very low x. (b) Saturation scale. the hatched area defines a prediction band of Ref. [37]; dashed line is the GBW model.

Model predictions for F_L at HERA and F_2 at LHC can be found in Ref. [37]. Having determined the dipole cross section we can relate it to the unintegrated gluon distribution $f(k,y)$:

$$\sigma^{dipole}(r,y) = \frac{4\pi^2}{N_c} \int \frac{d\,k^2}{k^4} \left[1 - J_0(k\,r) \right] \alpha_s(k^2)\, f(k,y).$$ (4)

The relation (4) can be inverted for f which can be then used as an input for any computation based on the k_t factorization scheme. The data set for the dipole cross section σ^{dipole} as well as for the unintegrated gluon f can be found in [24]. The uPDF is compared to other parameterizations in Fig.1.

3.3 Outlook

We have reported on, so far, the most advanced analysis of the F_2 data based on combined BK/DGLAP evolution equations. Though our approach incorporates most of the knowledge accumulated in saturation physics, it is not yet fully developed. The next essential steps would be to include NLO corrections both to BFKL and DGLAP. The quark sector should be also added into a unique scheme.
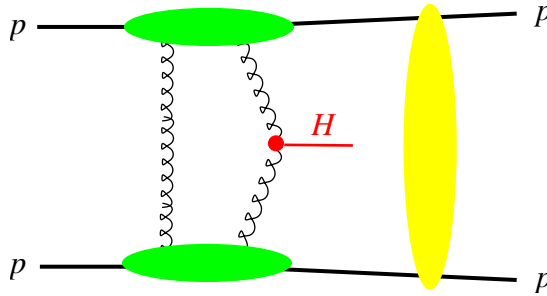
4 Generalized parton distributions[5]

The theoretical description of hard diffractive processes involves the gluon distribution in the proton. Such processes have a proton in the final state which carries almost the same momentum as the incident proton. Due to the small but finite momentum transfer, it is not the usual gluon distribution which appears, but its generalization to nonforward kinematics. Prominent example processes are the exclusive production of mesons from real or virtual photons (Figure 12a) when either the photon virtuality or the meson mass provides a hard scale, virtual Compton scattering $\gamma^* p \to \gamma p$, and the diffractive production of a quark-antiquark pair (Figure 12b) in suitable kinematics. The generalized gluon distribution depends on the longitudinal momentum fractions x and x' of the emitted and reabsorbed gluon (which differ because of the longitudinal momentum transfer to the proton) and on the invariant momentum transfer $t = -(p - p')^2$. In its "unintegrated" form it depends in addition on the transverse momentum k_t of the

---

[5]Authors: Markus Diehl and Thomas Teubner.
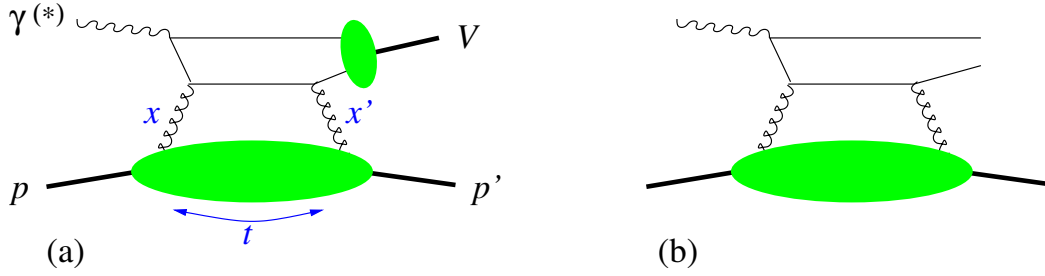
Fig. 12: Example graphs for the diffractive production of (a) a vector meson V or (b) a quark-antiquark pair. The large blob denotes the generalized gluon distribution of the proton and the small one the vector meson wave function.


Fig. 13: Graph for the exclusive diffractive production of a Higgs boson, $p + p \to p + H + p$. The horizontal blobs indicate generalized gluon distributions, and the vertical blob represents secondary interactions between the projectiles.

emitted gluon. Another important process involving this distribution is exclusive diffractive production of a Higgs in pp scattering (Figure 13), discussed in detail in [41]. Note that the description of this process requires the gluon distribution to be unintegrated with respect to k_t, whereas the processes in $\gamma^{(*)}p$ collisions mentioned above can be treated either in k_t-factorization or in the collinear factorization framework, where k_t-integrated generalized parton distributions occur. Note also that Figures 12 and 13 show graphs for the process *amplitudes*: the cross section depends hence on the square of the gluon distribution for Figure 12, and on its fourth power for Figure 13.

To extract the generalized gluon distribution from vector meson production data requires knowledge of the meson wave function, which is an important source of uncertainty for the ρ^0 and ϕ and, to a lesser extent, for the J/Ψ. In this respect Υ production is by far the cleanest channel but experimentally challenging because of its relatively low production rate. An approach due to Martin, Ryskin and Teubner (MRT) [42] circumvents the use of the meson wave function by appealing to local parton-hadron duality, where the meson production cross section is obtained from the one for open quark-antiquark production, integrated over an interval of the invariant $q\bar{q}$ mass around the meson mass. The choice of that interval is then mainly reflected in an uncertainty in the overall normalization of the cross section. Virtual Compton scattering $\gamma^*p \to \gamma p$ does not involve any meson wave function and for sufficiently large Q^2 is again theoretically very clean.

By a series of steps one can relate the generalized gluon distribution to the usual gluon density, obtained for instance in global parton distribution fits.

1. The t dependence is typically parameterized by multiplying the distribution at $t = 0$ with an exponential $\exp(-b|t|)$, whose slope b has to be determined from measurement. In more refined models this slope parameter may be taken to depend on the other kinematic variables of the process.
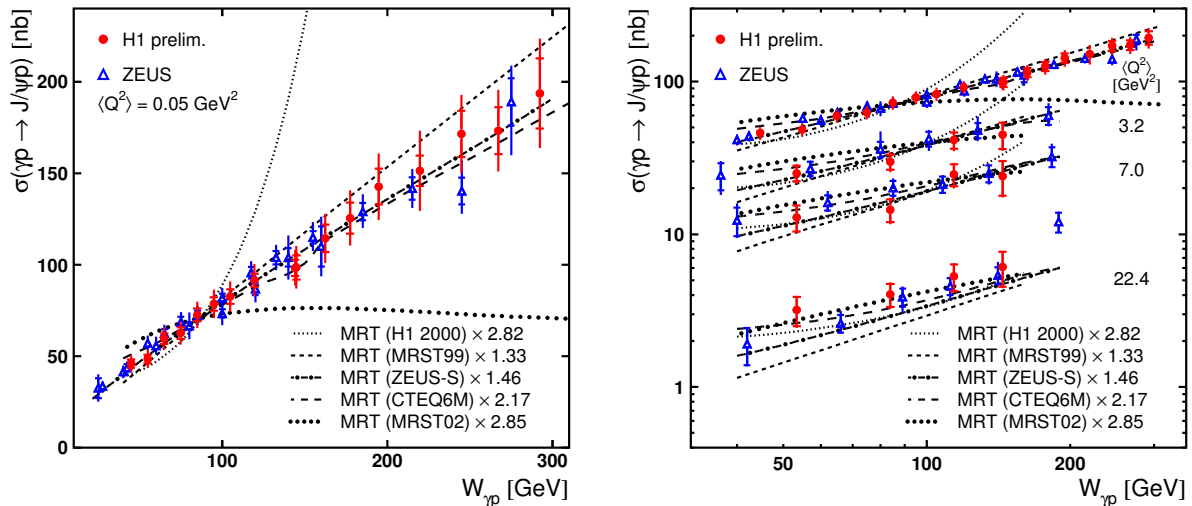
Fig. 14: Data for the $\gamma^* p \to J/\Psi\, p$ cross section from H1 [47] and ZEUS [48, 49] compared to calculations in the MRT approach [42, 46] with different gluon densities. The upper data points in the right panel correspond to those in the left one. The ZEUS data has been shifted to the Q^2 values of the H1 analysis using the Q^2 dependence measured by ZEUS, as described in [47]. Figure courtesy of Philipp Fleischmann (H1 Collaboration).

2. To leading logarithmic accuracy in $\log(1/x)$ one can neglect the difference between the longitudinal momentum fractions of the two gluons. The amplitude for meson production is then proportional to the usual gluon density evaluated at $x_g = (M_V^2 + Q^2)/W^2$, where M_V is the meson mass, Q^2 the photon virtuality, and W the $\gamma^* p$ c.m. energy. For phenomenology this leading logarithmic approximation is however insufficient. A weaker approximation allows one to express the amplitude in terms of the gluon density at x_g times a correction factor for the kinematic asymmetry ("skewing") between the two momentum fractions [43].

3. The problem to relate the k_t unintegrated gluon distribution to the k_t integrated one is quite analogous to the case of the usual forward gluon density (see Sect. 1.1), with some specifics concerning Sudakov form factors in the nonforward case [44].

An overview and discussion of theoretical aspects and uncertainties in describing vector meson production in this framework can be found in [45].

To illustrate the sensitivity of such processes to the gluon distribution we show in Figure 14 data for photo- and electroproduction of J/Ψ compared to calculations in the MRT approach [46], with different gluon densities taken as input to construct the generalized gluon distribution as just described. The potential of such processes to constrain the gluon distribution is evident from this plot.

We finally note that the theoretical description of diffractive Higgs production in pp collisions is very similar to the description of diffractive processes in ep scattering using k_t factorization (much more than to the description of, say, inclusive DIS in collinear factorization, which provides the main input to the determination of conventional gluon densities at small x), see [41, 50] for further discussion. The analysis of diffractive ep scattering is hence well suited to provide input to estimate the diffractive Higgs cross section at the LHC.

Acknowledgments

References

[1] V. Gribov and L. Lipatov, Sov. J. Nucl. Phys. **15**, 438 and 675 (1972).

[2] L. Lipatov, Sov. J. Nucl. Phys. **20**, 94 (1975).

[3] G. Altarelli and G. Parisi, Nucl. Phys. **B 126**, 298 (1977).

[4] Y. Dokshitser, Sov. Phys. JETP **46**, 641 (1977).

[5] E. Kuraev, L. Lipatov, and V. Fadin, Sov. Phys. JETP **44**, 443 (1976).

[6] E. Kuraev, L. Lipatov, and V. Fadin, Sov. Phys. JETP **45**, 199 (1977).

[7] Y. Balitskii and L. Lipatov, Sov. J. Nucl. Phys. **28**, 822 (1978).

[8] M. Ciafaloni, Nucl. Phys. **B 296**, 49 (1988).

[9] S. Catani, F. Fiorani, and G. Marchesini, Phys. Lett. **B 234**, 339 (1990).

[10] S. Catani, F. Fiorani, and G. Marchesini, Nucl. Phys. **B 336**, 18 (1990).

[11] G. Marchesini, Nucl. Phys. **B 445**, 49 (1995).

[12] L. Gribov, E. Levin, and M. Ryskin, Phys. Rep. **100**, 1 (1983).

[13] E. M. Levin, M. G. Ryskin, Y. M. Shabelski, and A. G. Shuvaev, Sov. J. Nucl. Phys. **53**, 657 (1991).

[14] S. Catani, M. Ciafaloni, and F. Hautmann, Nucl. Phys. **B 366**, 135 (1991).

[15] J. Collins and R. Ellis, Nucl. Phys. **B 360**, 3 (1991).

[16] J. C. Collins, D. E. Soper, and G. Sterman, Nucl. Phys. **B250**, 199 (1985).

[17] F. Landry, R. Brock, P. M. Nadolsky, and C. P. Yuan, Phys. Rev. **D67**, 073016 (2003). `hep-ph/0212159`.

[18] H. Jung and G. Salam, Eur. Phys. J. **C 19**, 351 (2001). `hep-ph/0012143`.

[19] H. Jung, *Un-integrated updfs in ccfm*, 2004. `hep-ph/0411287`.

[20] L. Lonnblad and M. Sjodahl, JHEP **05**, 038 (2005). `hep-ph/0412111`.

[21] B. Andersson, G. Gustafson, and J. Samuelsson, Nucl. Phys. **B467**, 443 (1996);
B. Andersson, G. Gustafson, and H. Kharraziha, Phys. Rev. **D57**, 5543 (1998). `hep-ph/9711403`.

[22] H. Jung, K. Kutak, K. Peters, and L. Motyka, *Nonlinear gluon evolution and heavy quark production at the lhc*. These proceedings, 2005.

[23] K. Kutak and A. M. Stasto, Eur. Phys. J. **C41**, 343 (2005). `hep-ph/0408117`.

[24] M. Lublinsky, *Parameterization of the dipole cross section and updf.* `http://www.desy.de/~lublinm/`.

[25] M. A. Kimber, A. D. Martin, and M. G. Ryskin, Phys. Rev. **D63**, 114027 (2001). `hep-ph/0101348`.

[26] H. Jung, Comput. Phys. Commun. **143**, 100 (2002). `hep-ph/0109102`.

[27] H. Jung and G. P. Salam, Eur. Phys. J. **C19**, 351 (2001). `hep-ph/0012143`.

[28] G. Watt, A. D. Martin, and M. G. Ryskin, Eur. Phys. J. **C31**, 73 (2003). `hep-ph/0306169`.

[29] G. Watt, A. D. Martin, and M. G. Ryskin, Phys. Rev. **D70**, 014012 (2004). `hep-ph/0309096`.

[30] J. C. Collins and X. Zu, JHEP **03**, 059 (2005). `hep-ph/0411332`.

[31] J. Kwiecinski, A. D. Martin, and J. J. Outhwaite, Eur. Phys. J. **C9**, 611 (1999). `hep-ph/9903439`.

[32] J. C. Collins, Acta Phys. Polon. **B34**, 3103 (2003). `hep-ph/0304122`.

[33] J. Bartels, Z. Phys. **C60**, 471 (1993);
J. Bartels, Phys. Lett. **B298**, 204 (1993);
E. M. Levin, M. G. Ryskin, and A. G. Shuvaev, Nucl. Phys. **B387**, 589 (1992).

[34] I. Balitsky, Nucl. Phys. **B 463**, 99 (1996).

[35] Y. V. Kovchegov, Phys. Rev. **D 60**, 034008 (1999).

[36] M. Lublinsky, E. Gotsman, E. Levin, and U. Maor, Nucl. Phys **A 696**, 851 (2001).

[37] E. Gotsman, E. Levin, M. Lublinsky, and U. Maor, Eur. Phys. J. **C 27**, 411 (2003).

[38] M. Lublinsky, Eur. Phys. J. **C 21**, 513 (2001).

[39] A. M. Stasto, K. Golec-Biernat, and J. Kwiecinski, Phys. Rev. Lett. **86**, 596 (2001).

[40] K. Golec-Biernat and M. Wusthoff, Phys. Rev. **D 59**, 014017 (1999).

[41] J. Forshaw, *Diffractive higgs production: theory*. These proceedings.

[42] A. D. Martin, M. G. Ryskin, and T. Teubner, Phys. Rev. **D55**, 4329 (1997). `hep-ph/9609448`;
A. D. Martin, M. G. Ryskin, and T. Teubner, Phys. Lett. **B454**, 339 (1999). `hep-ph/9901420`;
A. D. Martin, M. G. Ryskin, and T. Teubner, Phys. Rev. **D62**, 014022 (2000). `hep-ph/9912551`.

[43] A. G. Shuvaev, K. J. Golec-Biernat, A. D. Martin, and M. G. Ryskin, Phys. Rev. **D60**, 014015 (1999). `hep-ph/9902410`.

[44] A. D. Martin and M. G. Ryskin, Phys. Rev. **D64**, 094017 (2001). `hep-ph/0107149`.

[45] M. Diehl, Phys. Rept. **388**, 41 (2003). `hep-ph/0307382`.

[46] T. Teubner. To appear in Proceedings of DIS05.

[47] H. C. A. Aktas et al., *Elastic J/Ψ production at HERA*. `hep-ex/0510016, Submitted to Eur Phys J`.

[48] ZEUS Collaboration, S. Chekanov *et al.*, Nucl. Phys. **B695**, 3 (2004). `hep-ex/0404008`.

[49] ZEUS Collaboration, S. Chekanov *et al.*, Eur. Phys. J. **C24**, 345 (2002). `hep-ex/0201043`;
ZEUS Collaboration, J. Breitweg *et al.*, Eur. Phys. J. **C6**, 603 (1999). `hep-ex/9808020`;
ZEUS Collaboration, J. Breitweg *et al.*, Z. Phys. **C75**, 215 (1997). `hep-ex/9704013`.

[50] L. Motyka, *Talk at the workshop meeting 7–21 January 2005, CERN*.
http://agenda.cern.ch/fullAgenda.php?ida=a045699;
M. Diehl, *Talk at the workshop meeting 21–24 March 2005, DESY*.
http://agenda.cern.ch/fullAgenda.php?ida=a05611.